# Gold-coated nanoripples produced by UV-Femtosecond lasers for surface enhanced Raman spectroscopy

Nan Li, Xi Huang, Haoyu Dong, Bin Duan, Qiuchi Zhu, Aofei Mao, Peizi Li, Bai Cui, Jean-Francois Silvain, Yongfeng Lu

# Gold-Coated Nanoripples Produced by UV-Femtosecond Lasers for Surface Enhanced Raman Spectroscopy

**Nan Li[1,#], Xi Huang[1,#,*], Haoyu Dong[1], Bin Duan[2,3,4], Qiuchi Zhu[1], Aofei Mao[1], Peizi Li[1], Bai Cui[4], Jean-Francois Silvain[5] , and Yongfeng Lu[1,*]**

[1]*Department of Electrical and Computer Engineering, University of Nebraska, Lincoln, NE 68588, USA.*

[2]*Mary & Dick Holland Regenerative Medicine Program, University of Nebraska Medical Center, Omaha, NE, USA*

[3]*Department of Surgery, College of Medicine, University of Nebraska Medical Center, Omaha, NE, USA*

[4]*Department of Mechanical and Materials Engineering, University of Nebraska, Lincoln, NE 68588, USA.*

[5]*CNRS, University of Bordeaux; Bordeaux I.N.P., ICMCB, UMR 5026, F-33608 Pessac, France.*

*#Nan Li and Xi Huang contributed equally to this work.*

**Corresponding authors:*

*Yongfeng Lu, E-mail address: ylu2@unl.edu*

*Xi Huang, E-mail address: huangxi.1989.u.s@gmail.com*

## Abstract

Femtosecond (fs) lasers have been recognized as a powerful tool for micro/nanofabrication, due to their advantages of high flexibility, high repeatability, and minimal introduction of heat. Many studies have been made to employ fs laser processing in fabrication of nanostructures on substrates for surface-enhanced Raman spectroscopy (SERS). However, there have been few reports of ultraviolet (UV)-fs-laser-induced nanoripples for SERS experiments. In this study, we developed simple, easy-to-prepare, and large-active-area SERS substrates using UV-fs laser irradiation. Nanoripples induced in open air by the UV-fs laser on Silicon (Si) substrates with gold

coatings were used as SERS-active substrates. Nanoripple evolution by the UV-fs laser was explored to establish the processing windows for nanoripple formation as functions of laser fluence and hatching distances. Moreover, SERS enhancement factors (EFs) were correlated with the laser induced nanoripple patterns. SERS EFs up to $2.4\times10^7$ were achieved for Rhodamine 6G (R6G) molecules on the laser-textured Si substrates with Au coatings of 34 nm thick. The average period of nanoripples for the highest SERS EF is 253 nm, fabricated by a laser fluence of 0.48 J/cm$^2$ and a hatching distance of 38 μm. R6G concentration down to $10^{-9}$ mol/L was detected on the laser-textured Si substrate. Besides Si substrates, three other materials, stainless steel, glass, and polystyrene, were also investigated for nanoripple formation and SERS measurements. Nanoripple structures were formed on stainless-steel surfaces and the highest SERS EF of $1.5\times10^7$ was achieved. For glass and polystyrene substrates, no nanoripple structures were found. As a result, the SERS EFs (~$10^6$) of glass and polystyrene are one order of magnitude lower than those of the Si and stainless-steel substrates. The SERS demonstration using these materials further supports the mechanisms of nanoripple formation and provides a foundation to make UV-fs laser processing an effective technique for SERS applications using various materials. Applications for Sudan I, sEVs, and glucose were explored and demonstrated the capability of the SERS substrates.

**Keywords:** UV Femtosecond laser, Nanoripples, SERS

## 1. Introduction

Since the first demonstration in the 1970s [1], the surface enhanced Raman scattering (SERS), with the ability of single-molecule detection [2], has been applied in various fields requiring high accuracy sensing, such as biosensing [3, 4], toxic molecules detection [5, 6], and explosive material detection [7, 8] and so on. In SERS, nanostructure arrays are usually important in generating hot spots, where optical fields are significantly enhanced due to the localized surface plasmon

resonance (LSPR). Researchers employed various approaches in the fabrication of nanostructure arrays for SERS applications, such as focused ion beam (FIB), self-organized nanopatterning with ion-beam assistance [9-11], ultrathin alumina mask (UTAM) surface pattern technique [12], chemical synthesis of nano-crystals [13], dendrites formation by galvanic displacement [14]. Despite certain merits of the above methods demonstrated for SERS applications, a technique with high flexibility, high sensibility, high repeatability, and low cost at the same time is always desired.

Femtosecond (fs) lasers have been recognized as a powerful tool for micro/nanofabrication, [15-18] due to their advantages of high flexibility, high repeatability, and minimal heat introduction. Fs laser processing has been employed in the fabrication of nanostructures on SERS substrates. Cao *et al.* [19] employed underwater fs-laser processing in the fabrication of Au nanoparticle-decorated nanorod arrays for SERS applications. Fu *et al.* [20] fabricated superhydrophobic nanostructures on copper as sensitive SERS substates by fs-laser ablation. Byram *et al.* [21] fabricated Au nanostructures on SERS substrates using fs-laser ablation in liquids. Buividas *et al.* [22] created nanoripples on sapphire substrates by fs-laser ablation and applied them as SERS substrates after Au coating. Chandu *et al.* [23] fabricated cage like nanostructures on Ni substrates by fs-laser ablation in liquids and demonstrated their SERS performance after Au coating. Ravi *et al.* [24] induced nanoripples on Si substrates via ps-laser ablation in acetone and investigated the SERS applications after gold coating. Luo *et al.* [25] investigated a one-step SERS-substrate fabrication by fs-laser ablation on a pure Ag plate in an Argon chamber. Ran *et al.* [26] explored the photosynthesis of Ag nanostructures by illuminating a fs-laser on Si substrates incubated in $AgNO_3$ solutions and employed the processed substrates for SERS applications. Li *et al.* [27] investigated the controllable Au-nanoparticle photoreduction by shaped fs-laser and explored SERS applications of this technique. Naqvi *et al.* [28] employed fs-laser ablation in the

preparation of hierarchical silver-nanoparticle/graphene-oxide hybrid structures and investigated their SERS response towards explosive materials.

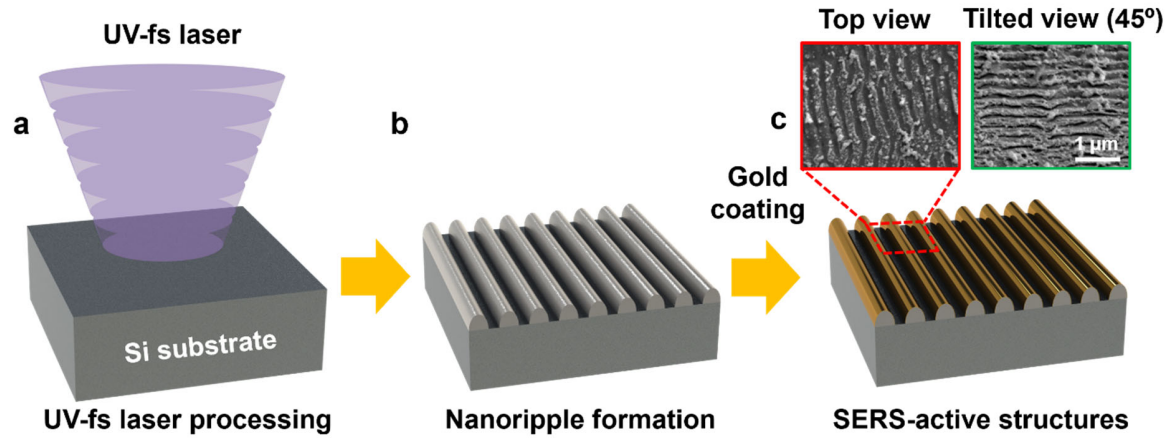


**Figure 1. Preparation of UV-fs-laser-textured Si substrates with 34 nm Au coatings. (a) UV-fs laser processing by changing hatching distances and laser fluences (Wavelength: 343 nm; pulse duration: 400 fs; pulse energy 48.3 μJ); (b) Formation of nanoripples on Si substrates; and (c) Au-coated Si substrates with nanoripples.**

In this study, we explored a simple, easy-to-prepare, and large-active-area ultraviolet (UV)-fs laser processing technique for SERS applications on various materials. Nanoripples fabricated by a UV-fs laser were used as the nanostructure arrays followed by the sputtering deposition of thin Au layers to act as SERS substrates, as shown in Figure 1. Silicon (Si) substrates were chosen as the primary test materials. Despite many studies have demonstrated the effectiveness of fs-laser processing in the fabrication of SERS substrates, there are few reports of UV-fs-laser-induced nanoripples for SERS experiments. In this work, we employed a UV-fs laser (343 nm) to induce nanoripple structures on material surfaces, such as Si surfaces. A thin layer of Au coating was then deposited on the formatted nanoripple structures. Rhodamine 6G (R6G) molecules with different concentrations ranging from $10^{-1}$ to $10^{-10}$ mol/L were measured using the SERS substrates to obtain

SERS enhancement factors (EFs). Sudan I, an organic dye, was also measured to demonstrate the capability of the substrates. This study 1) explores the nanoripple evolution by UV-fs lasers and confirms the processing windows for nanoripple formation as functions of hatching distance and laser fluence; and 2) correlates the SERS EFs and Au-coated UV-fs-laser-induced nanoripple patterns. The processing strategy of nanoripples has been demonstrated to be successful on semiconductor and conductor materials, such as Si and stainless-steel surfaces. Highest SERS EFs of $2.4\times10^7$ and $1.5\times10^7$ were achieved for R6G on UV-fs-laser-textured Si and stainless-steel substrates, respectively. R6G concentration down to $10^{-9}$ mol/L was detected on the laser-textured Si substrate. At the same time, no nanoripple structure was observed on surfaces of glass and polystyrene. The demonstration on these materials further supports the mechanisms of nanoripple formation and provide a foundation to make UV-fs laser processing an effective technique for SERS applications using various materials.

## 2. Experiments

### 2.1 Fabrication of SERS substrates

Substrates of four different materials, Si, stainless steel, glass, and polystyrene, were structured using the UV-fs laser system. The UV-fs laser (Tangor laser, Amplitude Laser Inc.) with a third harmonic generator (THG) was used to generate a wavelength of 343 nm. The maximum pulse energy of the UV-fs laser is 83 μJ. For UV-fs laser processing of Si, stainless steel, and polystyrene substrates, a pulse energy of 48.3 μJ was used. For UV-fs laser processing of glass substrates, a pulse energy of 83 μJ was used. The repetition rate was tuned to 330 kHz. The pulse duration of the UV-fs laser is 400 fs. The laser beam was scanned by a IntelliSCAN III 14 galvanometer scanner from SCANLAB GmbH. The laser beam was then focused by a f-theta lens with a 70 mm focal distance. The half divergence angle is estimated to be ~3.3º. In this study, the nanostructures

fabricated were studied as functions of laser fluence and hatching distance. The laser fluence is modulated by controlling the off-focal distance. The laser spot diameter ranged from 82 to 125 μm as the focal plane changed. The hatching distance between two adjacent laser scan lines was controlled as same as the distance between two consecutive laser pulses; Therefore, the hatching distance was controlled by the laser scanning speed and the laser repetition rate. For example, the hatching distance of 38 μm is determined by a scanning speed of 1 m/s and a repetition rate of 26 kHz. The laser fluence of 0.48 J/cm$^2$ is determined by the pulse energy of 48.3 μJ and an off-focal spot diameter of 113.6 μm. The size of the laser-treated area is 4×4 mm$^2$ on an 8×8 mm$^2$ Si substrate. To be noted, the laser-treated area depends on the scan field of the galvo scanner used. The SERS-active areas can be further increased than those demonstrated in this study. Besides UV wavelength, the Tangor laser system also can generate an IR laser beam at 1030 nm. The pulse energy of the IR-fs laser was set at 57.7 μJ (while the maximum pulse energy of the laser system is 265 μJ) and the same laser fluence (by tuning the off-focal distance) was used both for UV- and IR-fs laser processing. Thus, we compared the nanoripple formations and SERS performances using both UV and IR laser irradiation. After laser processing, Au layers were coated by a DC sputtering system (ATC ORION 5, AJA International) using a gold target (99.99% purity, Kurt J. Lesker Co.).

2.2 Characterization

The surface morphology was characterized using an FEI Helios Nanolab 660 dual-beam field-emission scanning electron microscope (SEM), which has a sub-nm resolution. Spatial periodicity and the height of nanoripples were measured from high-resolution cross-sectional SEM images of the nanoripples. R6G and Sudan I (Sigma-Aldrich, Inc.) were used for SERS experiments. High-purity methanol (VWR International, LLC.) was used as the solvent of R6G. High purity grade

acetone (VWR International, LLC.) was used as the solvent of Sudan I. All chemicals applied in this experiment are not further purified. The R6G concentrations of $10^{-1}$ to $10^{-10}$ mol/L and the Sudan I concentrations of $10^{-1}$ to $10^{-7}$ mol/L were prepared. One droplet (100 μL) of R6G or Sudan I solution was dropped on the prepared SERS substrates and measured after drying in the room temperature.

Raman spectra were acquired by a commercial Raman spectrometer (Renishaw inVia). A He-Ne laser (633 nm) with a power of 10 mW was used for the Raman excitation. A 50× microscope objective with a numerical aperture (NA) of 0.5 was used for the Raman spectrum acquisition. The exposure time for each spectrum was set to be 5 sec with a single accumulation. The data collected was recorded using the Wire 3.2 software. A six-order polynomial fit was used to remove the background of the Raman spectra collected by the Vancouver Raman Algorithm.

## 3. Results and Discussion

### 3.1 Nanoripples on Si substrates controlled by laser fluences and hatching distances

In this study, Si substates were chosen as the primary material for UV-fs laser processing and Au coating. Si substrates structured by UV-fs laser fluences of 0.39-0.91 J/cm$^2$ and hatching distances of 23-45 μm were coated with Au layers to serve as the SERS substrates. Figure 2 shows the SEM images of laser-structured Si substrates with Au coatings, which indicates the influences of the two main parameters, laser fluence and hatching distance, on the formation of the nanoripples. The laser fluence and hatching distance strongly influence the spatial/temporal distribution of laser energy, which determines the final surface morphology after laser processing [29]. The finest nanoripple structures with an average period of 226 nm were formatted with a laser fluence of 0.75 J/cm$^2$ and a hatching distance of 38 μm. Table 1 shows the averaged dimensions of UV-fs (343 nm) and Infrared (IR)-fs (1030 nm) laser-induced nanoripples (the

SERS comparison between UV and IR laser wavelengths will be detailed in Section 3.3). Figure S1 shows the SEM images of the cross-sections of nanoripples with 34 nm Au coatings.

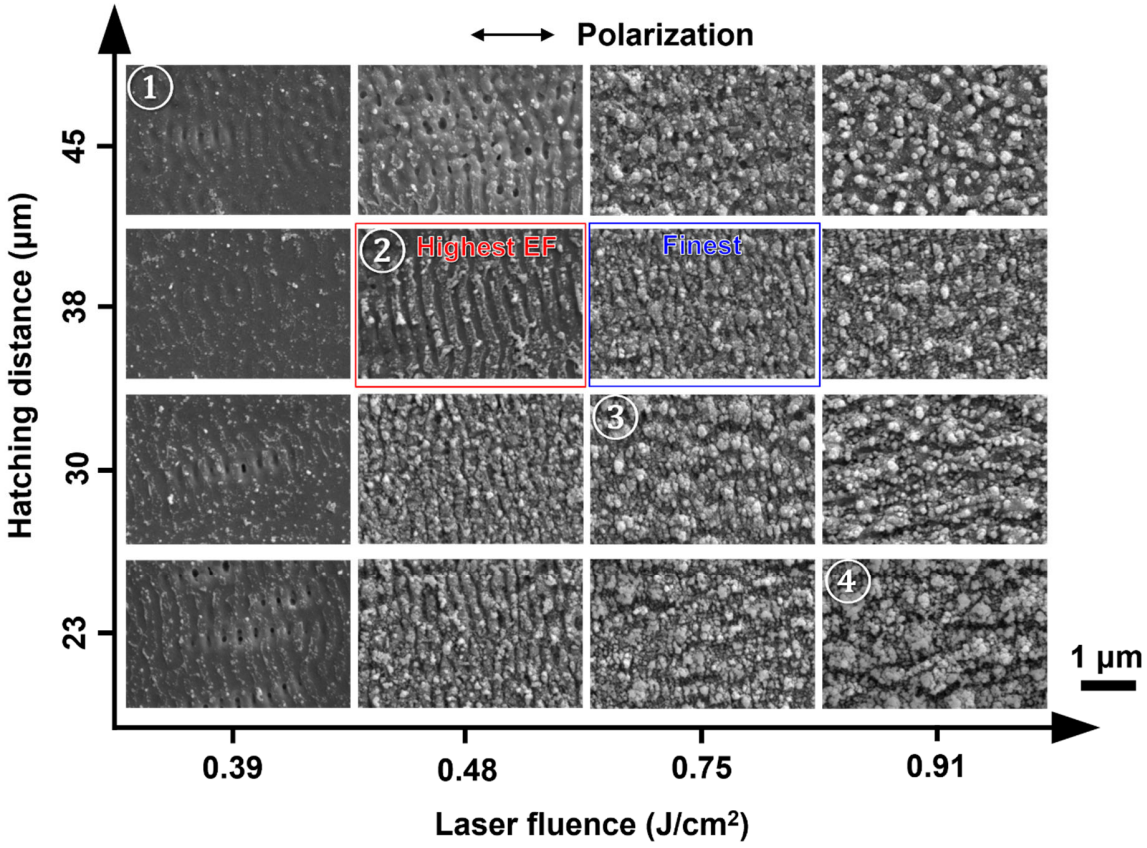


**Figure 2. SEM images of laser-textured Si substrates with Au coatings (thickness: 34 nm). The finest nanoripple structures with an average period of 226 nm were formed with a laser fluence of 0.75 J/cm$^2$ and a hatching distance of 38 μm. The nanoripple structures with an average period of 253 nm for the highest SERS EF of 2.4×10$^7$ were formed by a laser fluence of 0.48 J/cm$^2$ and a hatching distance of 38 μm. The laser polarization is perpendicular to the nanoripples.**

In our experiments, the finest nanoripple belongs to a low-spatial-frequency type of laser-induced periodic surface structure (LIPSS), which are oriented perpendicular to the laser beam polarization and exhibit periods related with the wavelength. According to Bonse *et al.* [30], low-

spatial-frequency LIPSS (LSFL) typically exhibit periods close to or slightly smaller than the irradiation wavelength ($0.5\lambda \leq$ LSFL periods $\leq \lambda$). The finest nanoripples in our experiment have a periodicity of 226 nm, which is equal to $0.66\lambda$ ($\lambda$ = 343 nm).

**Table 1 Averaged dimensions of UV- and IR-fs-laser-induced nanoripples as a function of laser fluences at a fixed hatching distance of 38 µm.**

| Wavelength (nm) | Fluence (J/cm$^2$) | Height (nm) | Periods (nm) |
|---|---|---|---|
| UV (343) | 0.39 | 84 | 302 |
| UV (343) | 0.48 | 123 | 253 |
| UV (343) | 0.75 | 110 | 226 |
| IR (1030) | 0.40 | 167 | 955 |
| IR (1030) | 0.92 | 262 | 930 |

The processing parameters significantly impact the formation of the nanoripples. As the laser fluence increases, the nanoripples evolve from continuous to discontinuous ripples (mixture of ripples and particles) and then eventually to particle-covered grooves. This morphology transition has been reported by Bonse *et al.* [31] and Wang *et al.* [32]. The transition mechanisms from nanoripples to particle-covered grooves could be attributed to an inhomogeneous nucleation and subsequent light redistribution [33]. When less laser fluences (<0.75 J/cm$^2$) were applied, nanoripple structures are clear to be observed. As the laser fluence was increased to 0.91 J/cm$^2$, the ripple structures start to disappear, and instead randomly distributed particles are formed together with horizontal grooves at microscales. The nanoripple surface processing was performed by a raster scan strategy using a galvo scanner. As the hatching distance decreases, the laser energy absorbed in a unit surface area increases, causing the LIPSS evolution from nanoripples to disordered grooves. When the laser fluence is 0.48 J/cm$^2$, the appropriate hatching distance (38

μm) results in the finest nanoripples. Either lower (23 and 30 μm) or higher (45 μm) hatching distance resulted in the discontinued ripple structures.

### 3.2 SERS on UV-fs-laser-textured Si substrates with Au coatings

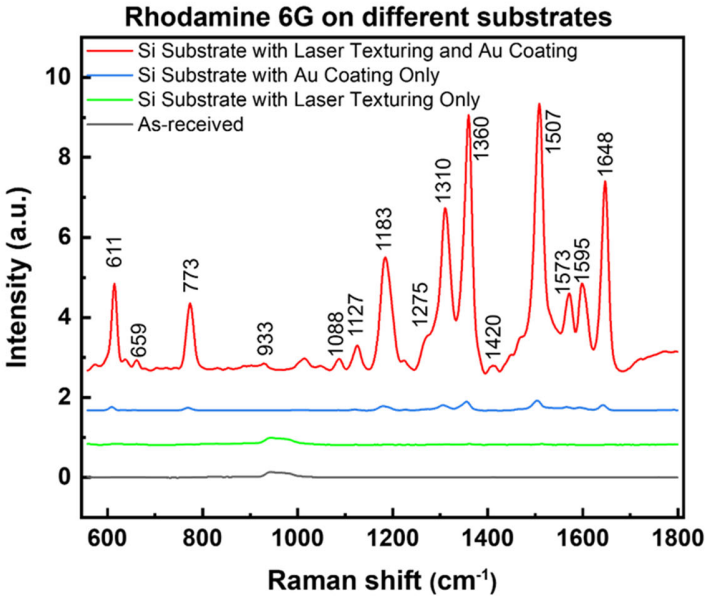


**Figure 3. Raman spectra of R6G molecules ($10^{-6}$ mol/L) on Si substrates (1) with laser texturing and Au coating; (2) with Au coating only; (3) with laser texturing only; and (4) as received. The wavelength of the processing fs laser is 343 nm. The wavelength of the Raman excitation laser is 633 nm.**

The Au coatings by sputtering deposition on the textured surfaces serve as a simple, convenient, and cost-effective way to provide localized surface plasmon resonance for SERS. Si was selected as the primary material for testing. The optimized thickness for the Au coatings was found to be 34 nm on the laser-textured Si substrates for the best enhancement factor (EF) of SERS (Figure S2). Raman spectra of R6G molecules acquired from the Au-coated textured Si substrates exhibit strong Raman lines at 611, 773, 1127, 1183, 1310, 1360, 1507, 1573, and 1648 $cm^{-1}$, as shown in

Table S1 [34]. 611 $cm^{-1}$ is the C-C-C ring in-plane bending vibration. 773 $cm^{-1}$ is the C-H out-of-plane bending vibration. 1127 $cm^{-1}$ is the C-H in-plane bending vibration. Peaks at 1310, 1360, 1507, 1573, and 1648 $cm^{-1}$ are assigned to the aromatic stretching vibrations. Raman spectra were corrected by subtracting a six-order polynomial fitting curve of fluorescence backgrounds by the Vancouver Raman Algorithm. As shown in Figure 3, there is no R6G signal on as-received Si and UV-fs-laser-textured Si substrates without Au coatings. The band in the range of 935-990 $cm^{-1}$ comes from $SiO_2$ films naturally formed on the Si substrates. As a comparison, we placed R6G on Si substrates with 34 nm Au coatings, and some Raman peaks of R6G were observed in the spectrum. When we placed R6G on the UV-fs-laser-textured Si substrates with 34 nm Au coatings, the Raman signals of R6G were significantly enhanced, to the extent that all the reported peaks of R6G were observed through the spectrum. At the same time, there is no $SiO_2$ band in the spectra with Au coatings, which indicates the Au coating may suppress the background signals from the substrates.

The diameter of the laser focal spot used for Raman excitation (633 nm) is estimated to be ~ 1.5 μm when focused by a long working distance 50× objective (0.5 NA) for obtaining averaged signals of R6G from a few of periods of nanoripples formed on the Si substrates. The SERS EFs have been further studied. The intensities should be normalized for the acquisition time, laser power, and detector sensitivity. The enhancement factor (EF) is defined by

$$EF = \frac{I_{SERS}}{I_{ref}} \frac{C_{ref}}{C_{SERS}} \quad (1)$$

where $I_{ref}$ and $I_{SERS}$ are the Raman peak intensities obtained on as-received Si substrates and SERS-active substrates with Au coatings; $C_{ref}$ and $C_{SERS}$ are the R6G concentrations used for obtaining $I_{ref}$ and $I_{SERS}$ [35-37]. The Raman spectra of R6G on the as-received Si substrates were

selected as the reference. The concentrations of R6G used for the measurements of reference and SERS-active Raman spectra are $10^{-1}$ and $10^{-6}$ mol/L, respectively. The peak intensities at 1507 $cm^{-1}$ after background subtraction for reference and SERS-active substrates are $I_{ref}$ = 276, $I_{SERS}$ = $6.69\times10^4$, respectively. Therefore, the highest SERS EF of $2.4\times10^7$ was obtained, indicating an excellent SERS performance of the UV-fs-laser-textured Si with a 34 nm Au coating.

Figure 4(a) shows the SERS EF contour map of the Au-coated laser-textured Si substrates. The SERS EFs range from ~$10^5$ to ~$10^7$ as functions of laser fluence and hatching distance. The highest SERS EF of $2.4\times10^7$ is achieved on the optimized laser-textured Si substrates, which were processed with a laser fluence of 0.48 J/$cm^2$ and a hatching distance of 38 μm. The averaged period under the optimized processing parameters for the highest SERS EF is 253 nm. It is worth noting that the finest nanoripple structure (period = 226 nm) didn't result in the highest EF, because of the relatively low spatial uniformity. Figure 4(b) shows the comparison of typical Raman spectra of R6G ($10^{-6}$ mol/L) obtained from the laser-textured Si substrates. As we can see, the Raman features of R6G are significantly enhanced on the optimized laser-textured Si substrates. The SEM images of the spectra were labeled as 1-4 in Figure 2. All the Raman spectra of R6G ($10^{-6}$ mol/L) on Au-coated UV-fs-laser-structured Si substrates prepared as functions of laser fluence and hatching distance are shown in Figure S3. We also studied the Raman intensity changes of R6G as a function of R6G concentrations, as shown in Figure S4. R6G concentration down to $10^{-9}$ mol/L was detected on the laser-textured Si substrate. SERS EFs as a function of the angle between the polarization of the Raman excitation laser and the orientation of the formed nanoripples is shown in Figure S5, which indicates that the SERS EF is not sensitive to the polarization direction of Raman excitation laser. The highest EF reaches ~$2.4\times10^7$ when the polarization of the Raman excitation laser is parallel to the nanoripple orientation. The EF reaches a minimum of ~$2.1\times10^7$,

when the polarization of the Raman excitation laser and the nanoripple orientation are perpendicular to each other.

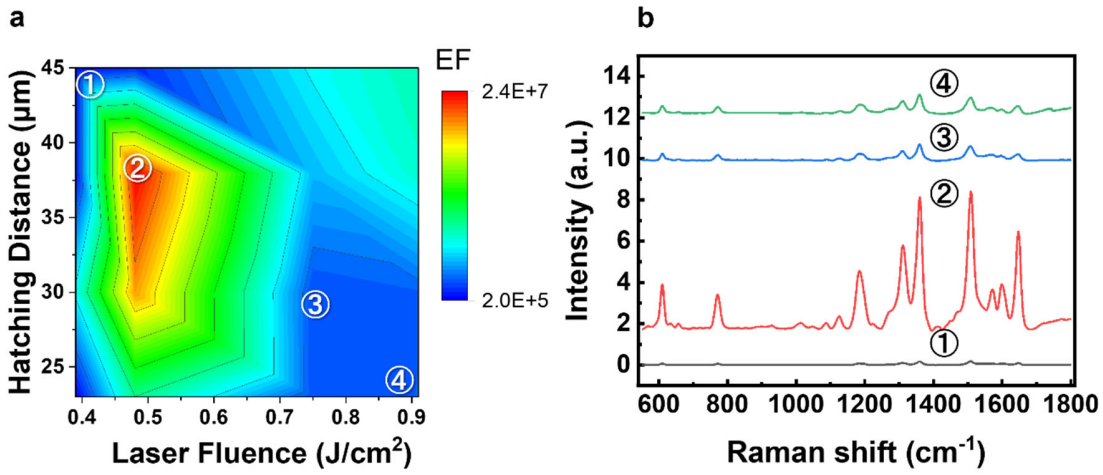


**Figure 4. (a) SERS EF Contour map of Au-coated (34 nm) laser-textured Si substrates. The highest SERS EF of $2.4\times10^7$ is achieved; (b) the typical Raman spectra 1-4 of R6G molecules ($10^{-6}$ mol/L) chosen from the contour map. The corresponding SEM images of the spectra 1-4 were shown in Figure 2. The wavelength of the processing fs laser is 343 nm.**

### 3.3 SERS comparison of UV- and IR-fs-laser-textured Si substrates with Au coatings

Figure 5 compares the SERS performances between the UV- and IR-fs-laser-textured Si substrates with Au coatings (34 nm). After repeating the optimization of IR laser processing, the highest SERS EF is found to be $3.3\times10^6$, one order of magnitude lower than the SERS samples textured by the UV-fs laser. The typical SEM images of the nanoripples fabricated by both UV and IR lasers for the highest SERS EFs are also presented in Figures 5a and 5c, respectively. The average period of nanoripples textured by the IR laser is 930 nm with a laser fluence of 0.92 J/cm$^2$ and a hatching distance of 38 μm. The comparison suggests that UV-fs-laser-induced nanoripples have better SERS performances due to the finer nanoripple structures (253 *vs* 930 nm). All the

Raman spectra of R6G ($10^{-6}$ mol/L) on Au-coated IR-fs-laser-structured Si substrates prepared as the functions of laser fluence and hatching distance are shown in Figure S6.

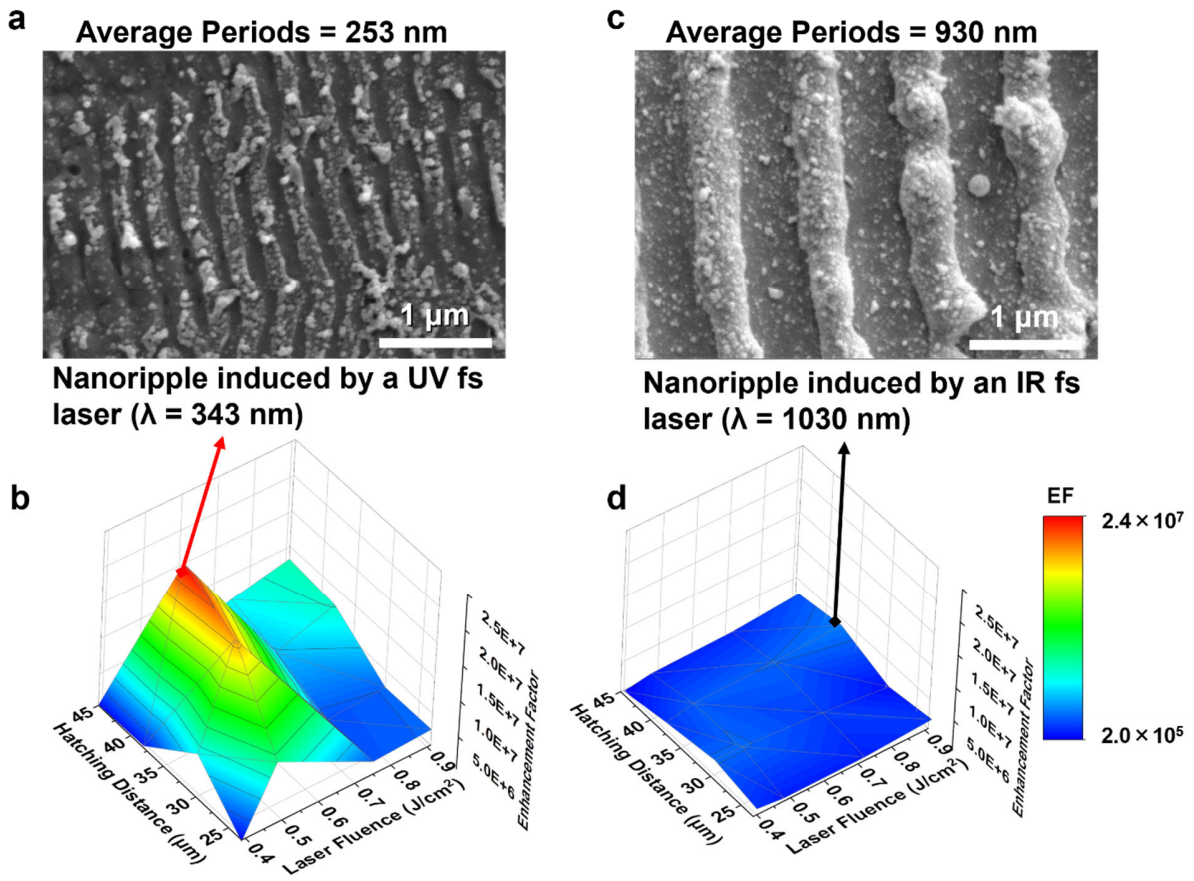


**Figure 5 SEM images and 3D SERS EF contour maps of (a)(b) UV- and (c)(d) IR-fs-laser-textured Si substrates with Au coatings (34 nm). The R6G concentration was $10^{-6}$ mol/L.**

### 3.4 Mechanisms of laser-induced nanoripples on conductors, semiconductors, and insulators

To our best understanding, strong absorbing materials, such as semiconductors and metals, the mechanism of nanoripple formation is based on surface plasmon polaritons (SPPs) [30]. The typical exhibit periods are close to or slightly smaller than the laser wavelength. The mechanism

involves the scattering of the incident electromagnetic wave at the rough surface, which leads to the excitation of SPPs, as shown in Figure 6a. Conductors directly provide free elections for SPP excitation leading to the formation of nanoripple structures, as shown in Figure 6b. Depending on the photon energy and the bandgap energy of the materials, irradiation with fs laser pulses on materials such as dielectrics and semiconductors can transiently be turned into a metallic state, which triggers the excitation of SPPs, as shown in Figure 6c. For dielectrics or insulators, such as glass or plastics, when the single-photon energy is smaller than the bandgap energy, it seems to be difficult for nanoripple formation based on our experimental results, as shown in Figure S7. Nanoripple formation experiments have been conducted on glass and polystyrene substrates. There is no nanoripple structure induced both on glass and polystyrene substrates at various hatching distances and laser fluences, although we still can detect R6G ($10^{-6}$ mol/L) with the highest SERS EFs of $2.2\times10^{-6}$ and $2.0\times10^{-6}$ on glass and polystyrene substrates, respectively. To be noted, the energy per pulse used here for glass is 83 μJ (the highest pulse energy of the laser system). The laser fluence used was sufficient for optical breakdown of the glass, since marks of laser ablation were observed on the glass surface after UV-fs laser processing. For polystyrene substrates, laser energy was set to 48.3 μJ. As a comparison, we repeated and optimized the UV-fs laser fabrication on stainless steel surfaces. The highest SERS EF of the UV-fs-laser-textured stainless-steel substrates is $1.5\times10^{7}$. All the Raman spectra of R6G ($10^{-6}$ mol/L) on Au-coated UV-fs-laser-structured stainless-steel substrates prepared as functions of laser fluence and hatching distance are shown in Figure S8. The pulse energy used for the stainless-steel substrates was set to 48.3 μJ. The typical SEM image of the UV-fs-laser-textured stainless-steel substrates for the highest SERS EF is shown in Figure 6e. The grain boundaries and UV-fs-laser-induced nanoripples on each grain are clearly observed. The optimized average period of stainless-steel for the highest SERS EF is

310 nm, which was prepared with a laser fluence of 2.39 J/cm$^2$ and a hatching distance of 45 µm. There is no R6G signal on as-received stainless-steel surfaces, but a significant SERS enhancement of R6G was observed on UV-fs-laser-textured stainless-steel surfaces with Au coatings. The results obtained from four different substrates, Si, stainless steel, glass, and polystyrene substrates further support the mechanisms of nanoripple formation. Through the study, Au-coated surfaces with UV-fs-laser-induced nanoripples demonstrate a higher SERS EF by at least one order of magnitude.

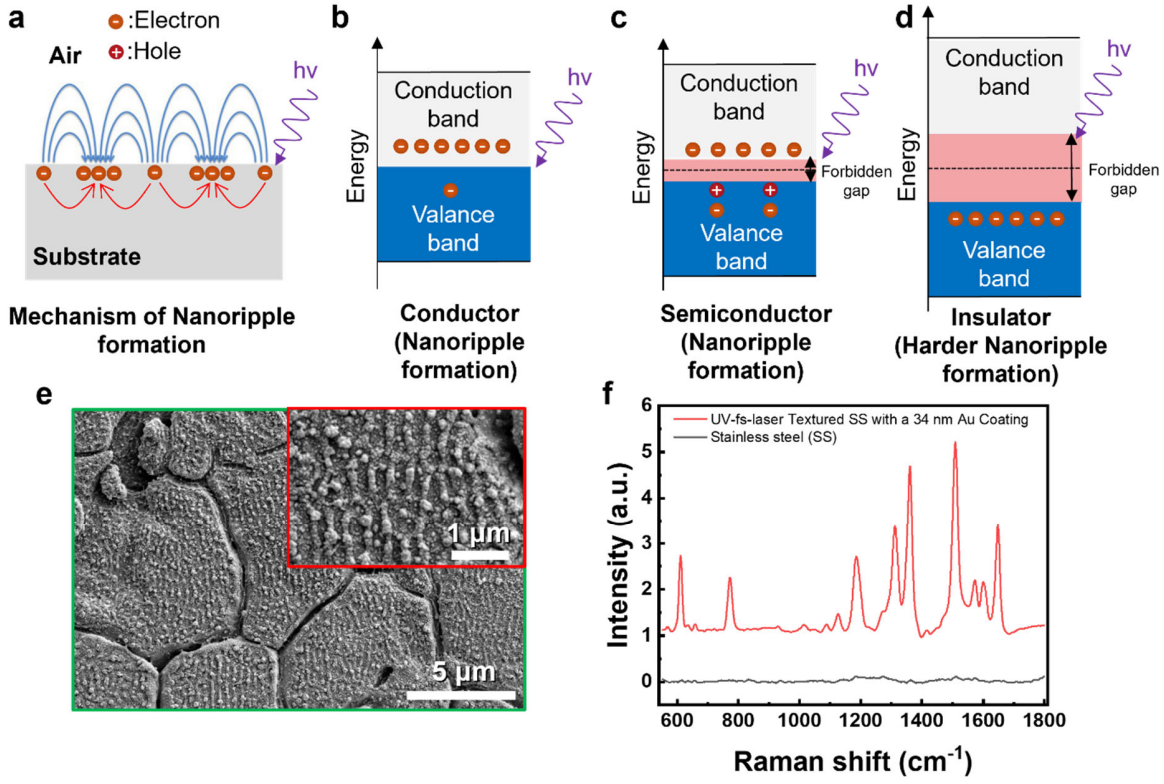


**Figure 6. (a) The mechanisms of nanoripple formation; (b) (c) Conductors and semiconductors provide free electrons and excited electrons for nanoripple formation; (d) Valance electrons in insulators are bound which leads to harder nanoripple formation. (e) SEM images of laser-textured (343 nm) stainless-steel surfaces with Au coatings for the highest SERS EF of 1.5×10$^7$; and (f) Raman spectra of R6G (10$^{-6}$ mol/L) on Au-coated laser-**

**textured stainless-steel substrates. The surface state of this stainless steel is a mill finish, which has clear grains in the SEM image.**

### 3.5 SERS measurements of Sudan I.

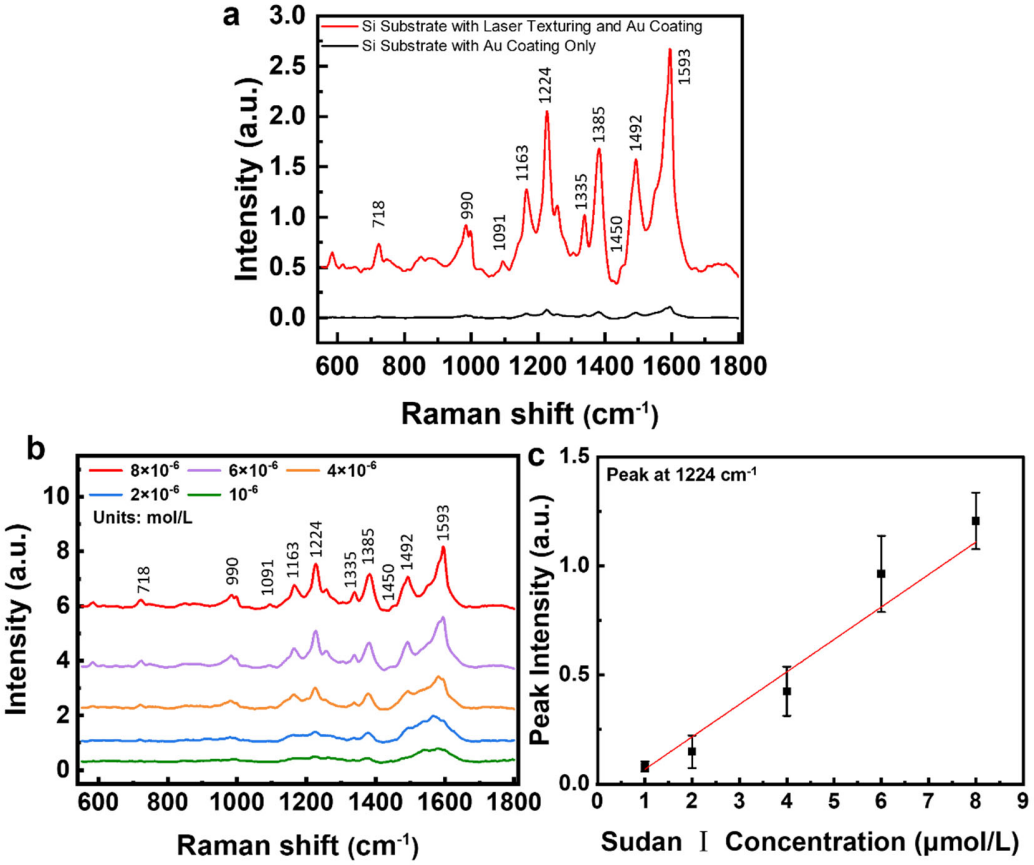


**Figure 7. (a) Raman spectra of Sudan I molecules ($8\times10^{-6}$ mol/L) on UV-fs-laser textured (343 nm) Si substrates with Au coating and untreated Si substrates with Au coating only; (b) Raman spectra and (c) Raman intensity as a function of concentration at the peak of 1224 $cm^{-1}$.**

Sudan I is an organic compound, which is an intensely orange-red powders that is added to colorize waxes, oils, petrol, solvents, and polishes. It also has been adopted for coloring various foodstuffs, such as curry powder and chili powder. Sudan I was measured to demonstrate the

capability of the SERS substrates which are UV-fs-laser textured Si substrates with 34 nm Au coatings. A comparison of UV-fs-laser-treated and untreated substrates on the detection of Sudan I molecules is shown in Figure 7(a). Besides, Raman spectra and intensities of Sudan I as functions of the concentration are shown in Figures 7(b) and (c). Raman spectra of Sudan I molecules acquired from the Au-coated textured Si substrates exhibit strong Raman lines at 718, 990, 1091, 1163, 1224, 1335, 1385, 1450, 1492 and 1593 $cm^{-1}$. The corresponding assignment of these Raman lines is shown in Table S2 [38]. The Raman intensities decrease as the function of Sudan I concentrations ranging from $10^{-5}$ to $10^{-6}$ mol/L. Some Raman peaks were still observable when the concentration of Sudan I was down to $10^{-6}$ mol/L. Therefore, the substrate is ideal for measurement of small molecules with a high enhancement factor.

### 3.6 SERS measurements of small extracellular vesicles (sEVs) and glucose

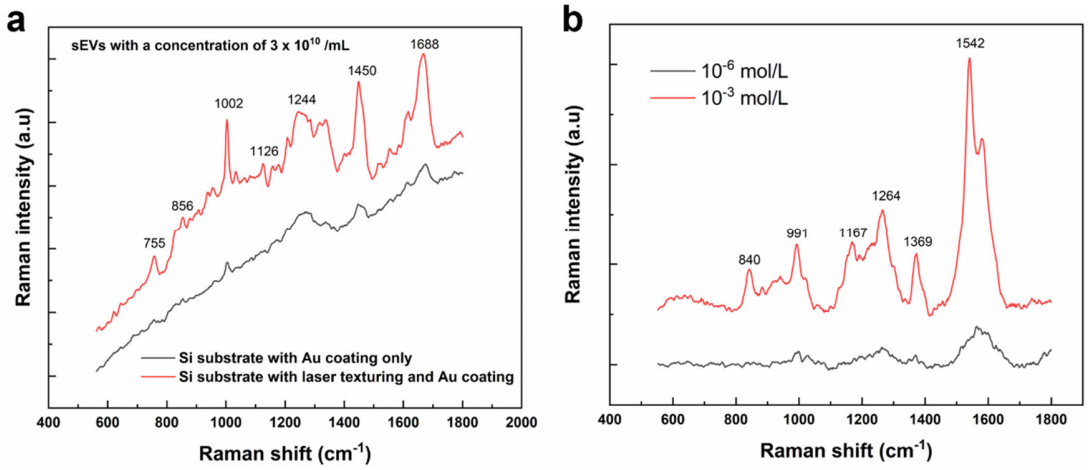


**Figure 8. Raman spectra of (a) sEVs on UV-fs-laser-textured (343 nm) Si substrates with Au coating and untreated Si substrates with Au coating only and (b) glucose with concentrations of $10^{-3}$ and $10^{-6}$ mol/L on UV-fs-laser textured (343 nm) Si substrates with Au coating.**

Small Extracellular vesicles (sEVs), which are small lipid-bilayer enveloped assemblies with sizes ranging from 20 nm to several micrometers, are found in most biological fluids and contain a wide variety of cargo, such as proteins, lipids, nucleic acids, and metabolites. These cargoes are representative of their cellular origin and reflective of the pathological condition of the origin tissue and cells, which may serve as noninvasive diagnostic biomarkers in biological fluids. In this study, Plasma-derived sEVs were isolated and prepared from human patient plasma related to coronary artery disease (CAD), which is detailed described in our previous work [39]. The typical size of the sEVs used in this study were 50-200 nm in diameter according to the results of nanoparticle tracking analysis (NTA) and the concentration of sEVs was $3\times10^{10}$/mL. The Raman spectra of sEVs acquired from the Au-coated textured Si substrates exhibit significantly enhanced Raman lines at 755 (symmetric ring breathing of tryptophan), 856 (glycogen), 1002 (phenylalanine), 1126 (C-C vibrations in lipid), 1244 (amide III), 1450 ($CH_2$ bending vibration of proteins/ lipids), and 1688 $cm^{-1}$ (amide I), in Figure 8 (a), which aligns with our previous studies [39]. To be noted, our nanoripple structures were optimized for the small molecules, R6G and Sudan I, which are organic compounds with low molecular weights ($\leqslant$1000 daltons) and sizes on the order of 1 nm; thus, when it comes to larger molecules such as sEVs, an optimization process on nanoripple is suggested. The future work will further optimize the two main parameters, laser fluence and hatching distance, for best SERS performance of sEVs. When combining advanced machine learning techniques, the optimized SERS substrates should have a great potential to serve as early diagnostic sensors of sEVs for various diseases, such as CAD [39] and lung cancer [40]. Besides the sEVs detection, another possible application by our SERS substrate was explored. Figure 8(b) shows a significant enhancement by our SERS substrates for glucose detection in mmol/L scale,

which indicates our substrate has a potential in blood glucose monitoring, which requires mmol/L accuracy [41].

## 4. Conclusion

This work explored the nanoripple evolution by UV-fs laser texturing and confirmed the processing windows for nanoripple formation as functions of laser fluence and hatching distance. SERS EFs were also correlated with the laser induced nanoripple patterns. Substrates were fabricated for SERS measurements with high EFs by two-step preparations (UV-fs laser processing in open air and Au sputtering). SERS EFs as high as $2.4\times10^7$ were achieved for R6G molecules on the UV-fs-laser-textured Si substrates with Au coatings of 34 nm. The average period of nanoripples with the highest EF is 253 nm, fabricated with a laser fluence of 0.48 J/cm$^2$ and a hatching distance of 38 μm. R6G concentration down to $10^{-9}$ mol/L was detected on the laser-textured Si substrate. Moreover, SERS EF is not sensitive to the polarization directions of the incident excitation laser. IR-fs laser was also applied to induce nanoripples on Si substrates with the SERS EFs one order of magnitude lower than those of the substrates textured by the UV-fs laser. Besides Si, other three materials, stainless steel, glass, and polystyrene were also investigated as the SERS substrates through the same parametric procedures. Nanoripple structures were able to be induced on stainless-steel surfaces with the highest SERS EF of $1.5\times10^7$. Conductors and semiconductors, such as Si and stainless steels tested in this work, are likely to form nanoripple structures under UV-fs laser irradiation; while insulators, such as glass and polystyrene, seem to be difficult to form nanoripples on surfaces. Through this study, Au-coated surfaces with UV-fs-laser-induced nanoripples demonstrate a higher SERS EF by at least one order of magnitude. The demonstrations of SERS on Si and stainless-steel substrates further support the mechanisms of nanoripple formation, and this study laid a foundation to make UV-fs laser processing an effective

technique for SERS applications on various materials. Applications for Sudan I, sEVs, and glucose were explored to demonstrate the capability of the SERS substrates.

## Acknowledgement

This study was supported by the National Science Foundation (CMMI 1826392) and the Nebraska Center for Energy Sciences Research (NCESR). The study was performed in part in the Nebraska Nanoscale Facility: National Nanotechnology Coordinated Infrastructure and the Nebraska Center for Materials and Nanoscience, which are supported by the National Science Foundation under Award ECCS: 1542182, and the Nebraska Research Initiative. The study was also partly performed at the NanoEngineering Research Core Facility (NERCF), which is partially funded by the Nebraska Research Initiative.

## References


1. M. Fleischmann, P. J. Hendra, and A. J. McQuillan, "Raman spectra of pyridine adsorbed at a silver electrode," Chemical Physics Letters **26**, 163-166 (1974).
2. K. Kneipp, Y. Wang, H. Kneipp, L. T. Perelman, I. Itzkan, R. R. Dasari, and M. S. Feld, "Single Molecule Detection Using Surface-Enhanced Raman Scattering (SERS)," Physical Review Letters **78**, 1667-1670 (1997).
3. Y. Yang, Y. Peng, C. Lin, L. Long, J. Hu, J. He, H. Zeng, Z. Huang, Z. Y. Li, M. Tanemura, J. Shi, J. R. Lombardi, and X. Luo, "Human ACE2-Functionalized Gold "Virus-Trap" Nanostructures for Accurate Capture of SARS-CoV-2 and Single-Virus SERS Detection," Nanomicro Lett **13**, 109 (2021).
4. K. C. Bantz, A. F. Meyer, N. J. Wittenberg, H. Im, Ö. Kurtuluş, S. H. Lee, N. C. Lindquist, S.-H. Oh, and C. L. Haynes, "Recent progress in SERS biosensing," Physical Chemistry Chemical Physics **13**, 11551-11567 (2011).
5. H. Wei, Z. Peng, C. Yang, Y. Tian, L. Sun, G. Wang, and M. Liu, "Three-Dimensional Au/Ag Nanoparticle/Crossed Carbon Nanotube SERS Substrate for the Detection of Mixed Toxic Molecules," Nanomaterials (Basel) **11** (2021).
6. D. J. Kim, S.-G. Park, D.-H. Kim, and S.-H. Kim, "SERS-Active-Charged Microgels for Size- and Charge-Selective Molecular Analysis of Complex Biological Samples," Small **14**, 1802520 (2018).
7. T. Liyanage, A. Rael, S. Shaffer, S. Zaidi, J. V. Goodpaster, and R. Sardar, "Fabrication of a self-assembled and flexible SERS nanosensor for explosive detection at parts-per-quadrillion levels from fingerprints," Analyst **143**, 2012-2022 (2018).
8. M. Liszewska, B. Bartosewicz, B. Budner, B. Nasiłowska, M. Szala, J. L. Weyher, I. Dzięcielewski, Z. Mierczyk, and B. J. Jankiewicz, "Evaluation of selected SERS substrates for trace detection of explosive materials using portable Raman systems," Vibrational Spectroscopy **100**, 79-85 (2019).
9. M. Ranjan, and S. Facsko, "Anisotropic surface enhanced Raman scattering in nanoparticle and nanowire arrays," Nanotechnology **23**, 485307 (2012).

10. M. Saini, S. Augustine, M. Ranjan, and T. Som, "In-plane optical anisotropy and SERS detection efficiency of self-organized gold nanoparticles on silicon nanoripples: Roles of growth angle and postgrowth annealing," Applied Surface Science **512** (2020).
11. K. P. Sooraj, M. Ranjan, R. Rao, and S. Mukherjee, "SERS based detection of glucose with lower concentration than blood glucose level using plasmonic nanoparticle arrays," Applied Surface Science **447**, 576-581 (2018).
12. Q. Fu, Z. Zhan, J. Dou, X. Zheng, R. Xu, M. Wu, and Y. Lei, "Highly Reproducible and Sensitive SERS Substrates with Ag Inter-Nanoparticle Gaps of 5 nm Fabricated by Ultrathin Aluminum Mask Technique," ACS Appl Mater Interfaces **7**, 13322-13328 (2015).
13. S. Tian, O. Neumann, M. J. McClain, X. Yang, L. Zhou, C. Zhang, P. Nordlander, and N. J. Halas, "Aluminum Nanocrystals: A Sustainable Substrate for Quantitative SERS-Based DNA Detection," Nano Letters **17**, 5071-5077 (2017).
14. A. Gutés, C. Carraro, and R. Maboudian, "Silver Dendrites from Galvanic Displacement on Commercial Aluminum Foil As an Effective SERS Substrate," Journal of the American Chemical Society **132**, 1476-1477 (2010).
15. D. Zhang, B. Ranjan, T. Tanaka, and K. Sugioka, "Underwater persistent bubble-assisted femtosecond laser ablation for hierarchical micro/nanostructuring," International Journal of Extreme Manufacturing **2** (2020).
16. P. Fan, B. Bai, M. Zhong, H. Zhang, J. Long, J. Han, W. Wang, and G. Jin, "General strategy toward dual-scale-controlled metallic micro-nano hybrid structures with ultralow reflectance," ACS Nano **11**, 7401-7408 (2017).
17. Y. Zhang, Y. Jiao, C. Li, C. Chen, J. Li, Y. Hu, D. Wu, and J. Chu, "Bioinspired micro/nanostructured surfaces prepared by femtosecond laser direct writing for multi-functional applications," International Journal of Extreme Manufacturing **2** (2020).
18. Y. Liu, W. Xiong, D. W. Li, Y. Lu, X. Huang, H. Liu, L. S. Fan, L. Jiang, J.-F. Silvain, and Y. F. Lu, "Precise assembly and joining of silver nanowires in three dimensions for highly conductive composite structures," International Journal of Extreme Manufacturing **1** (2019).
19. W. Cao, L. Jiang, J. Hu, A. Wang, X. Li, and Y. Lu, "Optical Field Enhancement in Au Nanoparticle-Decorated Nanorod Arrays Prepared by Femtosecond Laser and Their Tunable

Surface-Enhanced Raman Scattering Applications," ACS Appl Mater Interfaces **10**, 1297-1305 (2018).

20. P. Fu, X. Shi, F. Jiang, and X. Xu, "Superhydrophobic nanostructured copper substrate as sensitive SERS platform prepared by femtosecond laser pulses," Applied Surface Science **501** (2020).
21. C. Byram, S. S. B. Moram, A. K. Shaik, and V. R. Soma, "Versatile gold based SERS substrates fabricated by ultrafast laser ablation for sensing picric acid and ammonium nitrate," Chemical Physics Letters **685**, 103-107 (2017).
22. R. Buividas, P. R. Stoddart, and S. Juodkazis, "Laser fabricated ripple substrates for surface-enhanced Raman scattering," Annalen der Physik **524**, L5-L10 (2012).
23. B. Chandu, M. Sree Satya Bharati, P. Albrycht, and S. V. Rao, "Fabrication of nanocages on nickel using femtosecond laser ablation and trace level detection of malachite green and Nile blue dyes using surface enhanced Raman spectroscopic technique," Optics & Laser Technology **131** (2020).
24. R. K. Avasarala, T. Jena, S. K. Balivada, C. Angani, H. Syed, V. R. Soma, and G. K. Podagatlapalli, "Gold-coated silicon nanoripples achieved via picosecond laser ablation for surface enhanced Raman scattering studies," Results in Optics **5** (2021).
25. X. Luo, W. Liu, C. Chen, G. Jiang, X. Hu, H. Zhang, and M. Zhong, "Femtosecond laser micro-nano structured Ag SERS substrates with unique sensitivity, uniformity and stability for food safety evaluation," Optics & Laser Technology **139** (2021).
26. P. Ran, L. Jiang, X. Li, B. Li, P. Zuo, and Y. Lu, "Femtosecond Photon-Mediated Plasma Enhances Photosynthesis of Plasmonic Nanostructures and Their SERS Applications," Small **15**, e1804899 (2019).
27. C. Li, J. Hu, L. Jiang, C. Xu, X. Li, Y. Gao, and L. Qu, "Shaped femtosecond laser induced photoreduction for highly controllable Au nanoparticles based on localized field enhancement and their SERS applications," Nanophotonics **9**, 691-702 (2020).
28. T. K. Naqvi, M. Sree Satya Bharati, A. K. Srivastava, M. M. Kulkarni, A. M. Siddiqui, S. V. Rao, and P. K. Dwivedi, "Hierarchical Laser-Patterned Silver/Graphene Oxide Hybrid SERS Sensor for Explosive Detection," ACS Omega **4**, 17691-17701 (2019).

29. D. von der Linde, K. Sokolowski-Tinten, and J. Bialkowski, "Laser–solid interaction in the femtosecond time regime," Applied Surface Science **109-110**, 1-10 (1997).

30. J. Bonse, S. Hohm, S. V. Kirner, A. Rosenfeld, and J. Kruger, "Laser-Induced Periodic Surface Structures— A Scientific Evergreen," IEEE Journal of Selected Topics in Quantum Electronics **23** (2017).

31. J. Bonse, S. V. Kirner, M. Griepentrog, D. Spaltmann, and J. Krüger, "Femtosecond Laser Texturing of Surfaces for Tribological Applications," Materials **11**, 801 (2018).

32. A. Wang, L. Jiang, X. Li, Q. Xie, B. Li, Z. Wang, K. Du, and Y. Lu, "Low-adhesive superhydrophobic surface-enhanced Raman spectroscopy substrate fabricated by femtosecond laser ablation for ultratrace molecular detection," J Mater Chem B **5**, 777-784 (2017).

33. B. R. Tull, J. E. Carey, E. Mazur, J. P. McDonald, and S. M. Yalisove, "Silicon Surface Morphologies after Femtosecond Laser Irradiation," MRS Bulletin **31**, 626-633 (2006).

34. X. N. He, Y. Gao, M. Mahjouri-Samani, P. N. Black, J. Allen, M. Mitchell, W. Xiong, Y. S. Zhou, L. Jiang, and Y. F. Lu, "Surface-enhanced Raman spectroscopy using gold-coated horizontally aligned carbon nanotubes," Nanotechnology **23**, 205702 (2012).

35. L. Polavarapu, and Q.-H. Xu, "Water-Soluble Conjugated Polymer-Induced Self-Assembly of Gold Nanoparticles and Its Application to SERS," Langmuir **24**, 10608-10611 (2008).

36. C.-C. Chang, K.-H. Yang, Y.-C. Liu, T.-C. Hsu, and F.-D. Mai, "Surface-Enhanced Raman Scattering-Active Au/SiO2 Nanocomposites Prepared Using Sonoelectrochemical Pulse Deposition Methods," ACS Applied Materials & Interfaces **4**, 4700-4707 (2012).

37. Y. T. Lei, D. W. Li, T. C. Zhang, X. Huang, L. Liu, and Y. F. Lu, "One-step selective formation of silver nanoparticles on atomic layered MoS2 by laser-induced defect engineering and photoreduction," Journal of Materials Chemistry C **5**, 8883-8892 (2017).

38. C. Chen, F. Peng, Q. Cheng, and D. Xu, "Raman Spectra of Sudan Red Dyes and the Fluorescence Background Removal," in *2010 4th International Conference on Bioinformatics and Biomedical Engineering*(2010), pp. 1-4.

39. X. Huang, B. Liu, S. Guo, W. Guo, K. Liao, G. Hu, W. Shi, M. Kuss, M. J. Duryee, D. R. Anderson, Y. Lu, and B. Duan, "SERS spectroscopy with machine learning to analyze human plasma derived sEVs for coronary artery disease diagnosis and prognosis," Bioengineering & Translational Medicine **8**, e10420 (2023).

40. H. Shin, S. Oh, S. Hong, M. Kang, D. Kang, Y. G. Ji, B. H. Choi, K. W. Kang, H. Jeong, Y. Park, S. Hong, H. K. Kim, and Y. Choi, "Early-Stage Lung Cancer Diagnosis by Deep Learning-Based Spectroscopic Analysis of Circulating Exosomes," ACS Nano **14**, 5435-5444 (2020).

41. M. J. Scholtes-Timmerman, S. Bijlsma, M. J. Fokkert, R. Slingerland, and S. J. van Veen, "Raman spectroscopy as a promising tool for noninvasive point-of-care glucose monitoring," Journal of diabetes science and technology **8**, 974-979 (2014).